Inorganic Chemistry

pubs.acs.org/IC

Article

High-Pressure Polymorphism in Silver Ferrite Delafossite, $AgFeO_2$

Nicholas S. Manganaro, Scott D. Ambos, Matthew DeCapua, Scott D. Thiel, Wyatt E. Mitchell, Zhenxian Liu, Dongzhou Zhang, Phuong Q. H. Nguyen, Barbara Lavina, Esen Ercan Alp, Jun Yan,* and James P. S. Walsh*

Cite This: *Inorg. Chem.* 2024, 63, 9763−9770

Read Online

ACCESS | Metrics & More | Article Recommendations | Supporting Information

ABSTRACT: The delafossites are a class of layered metal oxides that are notable for being able to exhibit optical transparency alongside an in-plane electrical conductivity, making them promising platforms for the development of transparent conductive oxides. Pressure-induced polymorphism offers a direct method for altering the electrical and optical properties in this class, and although the copper delafossites have been studied extensively under pressure, the silver delafossites remain only partially studied. We report two new high-pressure polymorphs of silver ferrite delafossite, $AgFeO_2$, that are stabilized above ∼6 and ∼14 GPa. In situ X-ray diffraction and vibrational spectroscopy measurements are used to examine the structural changes across the two phase transitions. The high-pressure structure between 6 and 14 GPa is assigned as a monoclinic $C2/c$ structure that is analogous to the high-pressure phase reported for $AgGaO_2$. Nuclear resonant forward scattering reveals no change in the spin state or valence state at the Fe^{3+} site up to 15.3(5) GPa.

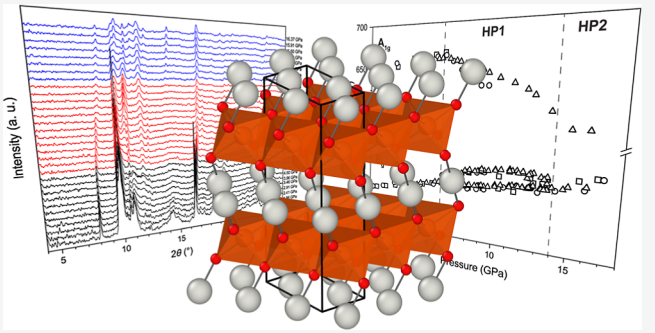

1. INTRODUCTION

The delafossites are a class of oxide materials that have attracted interest for a broad range of applications, including as water-splitting catalysts,[1] "metal-like" oxide conductors,[2] ionic charge carriers,[3,4] photovoltaics,[5] and optically transparent semiconductors.[6,7] The delafossites adopt the general formula ABO_2, where A is a monovalent transition metal cation and B is a trivalent transition or post-transition metal cation. The delafossite structure is remarkably flexible with respect to the cations that it can accommodate in the monovalent A site (Cu, Pd, Ag, and Pt) and trivalent B site (Al, Sc, Cr, Mn, Fe, Co, Ga, Rh, In, Tl, and Y). The delafossites are in many ways reminiscent of the perovskite oxides, not only in their remarkable flexibility with respect to the elements they can host but also in the similarity of their fundamental structural motif: the $\{BO_6\}$ octahedron. In the delafossites, the $\{BO_6\}$ octahedra adopt an edge-sharing connectivity to form two-dimensional oxide layers. These oxide layers are separated by A^+ ions, which form interactions with oxygen atoms in the adjacent layers. A number of delafossite polymorphs can form depending on the layer stacking sequence and the coordination of the interlayer A^+ ion, and sometimes the same empirical formula can express as multiple polymorphs.[8]

The delafossites can exhibit a broad range of bulk properties depending on which elements occupy the cation sites. For example, $PtCoO_2$ exhibits a remarkably low room temperature in-plane electrical resistivity of ∼2.1 $\mu\Omega$cm, which is not only low for an oxide but actually lower than that of many other conducting metals, including gold and aluminum.[9] In the copper and silver ferrite delafossites ($CuFeO_2$ and $AgFeO_2$), the band structure is semiconducting rather than metallic, allowing them to be used as photocathodes.[10] Another characteristic of delafossites that is of great interest to condensed matter physicists is their large electron mean free path lengths, which arise in part due to a very low defect concentration within their lattices.[11] The extended magnetic frustration that could arise from the triangular arrangement of the oxide layer ions also makes them an attractive testbed for investigating many fundamental aspects of magnetism.[12]

The structure of the 3R-polymorph of silver ferrite delafossite, $AgFeO_2$, is shown in Figure 1. This compound has been investigated for a range of potential applications, including as a cathode material in lithium-ion batteries,[4] as nontoxic and biocompatible semiconductor nanoparticles,[13] as components in solar energy conversion,[14] and as a host for multiferroic behavior.[15] Nanoparticles of $AgFeO_2$, which have a direct band gap of 2.0 eV, have also been investigated as

Received: December 29, 2023
Revised: April 9, 2024
Accepted: April 17, 2024
Published: May 13, 2024

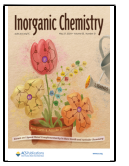

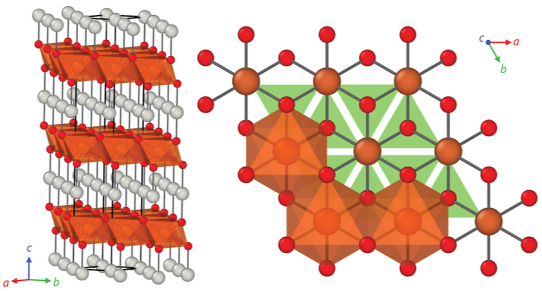

Figure 1. Left: crystal structure of 3R−$AgFeO_2$ viewed along the *ab*-plane. The {FeO_6} octahedra are rendered as 3 × 3 slabs of polyhedra (orange) to allow for clearer visualization of the stacking. Interlayer Ag^+ ions (gray) adopt a twofold linear O−Ag−O coordination with oxygen atoms (red) from the oxide layer. Right: top-down view of a 3 × 3 slab of the oxide layer. Polyhedra are rendered for three of the Fe atoms to illustrate the face-sharing connectivity. Green triangles highlight the triangular lattice formed by the oxo-bridged Fe atoms (orange).

magnetically guidable photocatalysts for the production of reactive oxygen species within cancer cells.[16]

Pressure is a powerful tool for smoothly modulating crystal structure to fine-tune structure-dependent properties and in many cases can be used to directly access different polymorphs with altered crystal symmetry and atomic connectivity. Although the copper delafossite systems have been well studied under pressure,[17−23] comparatively fewer studies have been carried out on the silver delafossites, and to date, only $AgGaO_2$ has been investigated with pressure.[24]

We present here the first experimental study of $AgFeO_2$ under high pressures. A suite of in situ techniques is used to characterize two previously unknown pressure-induced structural phase transitions that occur at ∼6 and ∼14 GPa.

2. EXPERIMENTAL SECTION

2.1. Synthesis of $AgFeO_2$. Ag_2O (0.4525 g, 99.99% metals basis, Alfa Aesar) and α-FeOOH (0.3496 g, 99+%, Alfa Aesar) were loaded into a 125 mL Teflon liner in a steel autoclave. To this, a solution of NaOH (19.4721 g) fully dissolved in deionized water (50 mL) was added with stirring. The reaction was heated from 25 °C at a rate of 70 °C per hour to 250 °C and held at this temperature for 120 h. It was then cooled at a rate of 6 °C per hour back down to 25 °C. NaOH was used to increase the solubility of both oxides.[8] The recovered product contained small hexagon-shaped single crystals along with iron oxide powder and some unreacted silver. Deep red hexagonal crystals were individually harvested from the product and washed with isopropanol. The hexagonal platelet single crystals ranged from 30−200 μm in width and 5−20 μm in thickness. X-ray diffraction (XRD) was used to determine whether crystals were of the 3R−$AgFeO_2$ or 2H−$AgFeO_2$ polymorph, with the former being much more common.

Samples for the nuclear resonant forward scattering (NRFS) were prepared with 40% enriched ^{57}Fe. A mixture of ^{57}Fe-enriched Fe_2O_3 (0.0407 g, 96.16% isotropic enrichment, IsoFlex) was mixed with nonenriched α-Fe_2O_3 (0.0610 g, 99+%, Alfa Aesar). The α−Fe_2O_3 mixture and Ag_2O (0.145 g, 99.99% metals basis, Alfa Aesar) were loaded into a 23 mL acid digestion vessel with 9.2 mL of water that had 2.234 g of NaOH dissolved in it. The same heating run profile as described above was used and produced crystals similar to the previous synthesis.

2.2. Vibrational Spectroscopy. A total of three Raman data sets and one far-infrared data set were collected at room temperature with increasing pressures up to ∼16 GPa. The first two Raman data sets and the far-IR data sets were collected at beamline 22-IR-1 at the National Synchrotron Light Source II (NSLS-II) at Brookhaven National Laboratory (BNL). The custom-made micro-Raman system includes an IsoPlane SCT-320 Imaging Spectrograph with a PyLon CCD detector (Princeton Instruments), a 300 μm 150 mW diode-pumped solid-state laser (Spectra-Physics), a beamsplitter, and a pair of SureBlock Ultra Narrow-band notch filters (Coherent). The laser wavelength was 488 nm. The far-IR setup included a Bruker Vertex 80 V spectrometer. The high-brightness synchrotron beam was used for infrared measurements of 100−680 cm^{-1} with 1 cm^{-1} resolution. The third Raman data set was collected in-house at UMass Amherst using a Horiba Jobin Yvon T64000 spectrometer in a single stage configuration (1800 lines/mm).

Hexagonal single crystals of 3R−$AgFeO_2$ (5−15 μm thick) were loaded individually along with two rubies into a symmetric-type diamond anvil cell (DAC) equipped with two diamonds (300 μm culets). Steel gaskets were indented to around ∼40 μm, and holes with a 210 μm diameter were drilled in the center of the indentation to create the sample chamber. For the two samples measured at BNL, petroleum jelly was used as the pressure transmitting media (PTM); for the data collected in-house at UMass Amherst, cryogenically loaded argon was used. Fluorescence from ruby spheres loaded in the sample space was used to determine pressure in all spectroscopy experiments.[25] Various PTM were used in this work. Table S5 tabulates the PTM used for each experiment, along with the hydrostatic limit where known. Errors for when specific pressures are reported depend on the PTM. For the gas media argon and neon, we report a 0.1 GPa error[26] and for experiments that used silicone oil and petroleum jelly, we report a conservative error of 0.5 GPa.[27] We were able to resolve both the R_1 and R_2 fluorescence lines from ruby up to the highest pressures measured with petroleum jelly, indicating that it remained at least quasi-hydrostatic over the measured range.

Temperature-dependent Raman spectra were also collected down to 5 K using a custom-built DAC designed to be mounted inside a Montana C2 cryostat. The PTM for these experiments was argon. A hexagonal single crystal identical to the ones loaded for the previously outlined experiments was loaded into the cell. The 5 mW diode-pumped solid-state laser had a wavelength of 532 nm. The DAC and gasket material, BeCu, and Re, respectively, were selected to be nonmagnetic to facilitate use inside a RTB superconducting magnet. Raman spectra were also collected at 0 GPa and 16.0(1) GPa under a 9 T out-of-plane field.

High-pressure synchrotron infrared spectroscopy was also performed at the NSLS-II. IR data were collected on the sample right after the Raman measurement was taken. After each Raman collection at the endstation of 22-IR-1B, the cells were moved to endstation 22-IR-1A for IR optical studies. The high-brightness synchrotron beam was used for far-infrared measurements of 100−680 cm^{-1} with 1 cm^{-1} resolution.

2.3. X-ray Diffraction. Cells were prepared using the same cell and anvil combinations as described for the Raman spectroscopy. Rhenium gaskets of 250 μm thickness were preindented to 40−50 μm. 210 μm diameter holes were then drilled into the center of the preindented area using a Boehler uDriller electrical discharge machining tool. For the single-crystal studies, a hexagonal single crystal (112 × 60 × 15 μm) that indexed to the 3R−$AgFeO_2$ polymorph was loaded into a DAC. Silicone oil was used as the PTM.

Single-crystal X-ray diffraction (SCXRD) was performed in-house using a Rigaku XtaLAB Synergy-S diffractometer equipped with a HyPix-6000HE detector. The DAC was mounted using a custom-made pin. X-rays were generated with a Ag-source (K_α = 0.56087 Å), and pressure was increased by tightening the bolts on the DAC by hand. Data were processed using CrysAlisPro software. Structural solution was prepared in Olex2[28] using the intrinsic phasing method within SHELXT.[29] Refinements of the model were performed using the least-squares method of SHELXL.[29]

For the powder X-ray diffraction (PXRD) experiment, we used two glass slides to crush 10 single crystals that had been individually indexed to the 3R−$AgFeO_2$ polymorph and then transferred the powder to the sample space of the gasket, which was prepared as described above for the single-crystal study. Neon was gas loaded as the PTM using the COMPRES user facility.[30] PXRD was performed

https://doi.org/10.1021/acs.inorgchem.3c04631
Inorg. Chem. 2024, 63, 9763−9770

at beamline 13-BM-C (GSECARS) at the Advanced Photon Source. At each pressure, diffraction was measured at the sample and then separately from a gold foil that was loaded into the sample space as a pressure calibrant.[31] Ruby fluorescence was also measured at each pressure. The pressure was increased using a gas membrane. X-rays were tuned to a wavelength of 0.434 Å. Diffraction was recorded using a Dectris Pilatus1M area detector. The incident X-ray beam was focused to a 12 × 18 μm^2 spot. A LaB_6 standard was used to calibrate detector positions. Integration of the images was performed with Dioptas.[32]

2.4. Nuclear Resonant Forward Scattering. NRFS was performed at Sector 3 at the Advanced Photon Source, Argonne National Laboratory. DACs were set up in the same way as those for Raman spectroscopy, as described above. A single crystal of ^{57}Fe-enriched $AgFeO_2$ with a thickness of 10 μm was loaded into the sample space along with two rubies that were used as pressure calibrants. Silicone oil was used as the PTM. A 14.4 keV beam was focused on an area of 15 × 15 μm^2 in the center of the sample. The pressure was increased incrementally using a gas membrane, and data were collected for 1−2 h at each pressure. A second run was performed on a thinner crystal (3 μm) from the same synthesis. To determine the isomer shift (δ), a ^{57}Fe-enriched stainless-steel disk was placed in the beam path. The resulting spectra were fitted with the CONUSS software package.[33]

2.5. Phonon Calculations. Density functional theory calculations were performed with CASTEP v23.1 using the "C19" library of ultrasoft pseudopotentials.[34] The *meta*-GGA regularized SCAN functional[35] and spin polarization in the ferromagnetic state were used to best match the experimental lattice parameters of the 3R−$AgFeO_2$ phase. The cutoff energy for the plane-wave basis set was 700 eV. Self-consistency was performed to an energy and force tolerance of 1 × 10^{-10} eV and 1 × 10^{-6} eV Å $^{-1}$, respectively. Structures were relaxed to a force tolerance of 0.001 eV Å $^{-1}$ prior to phonon calculations. The 3R−$AgFeO_2$ ($R\bar{3}m$) structure used a 14 × 14 × 14 Monkhorst−Pack *k*-point grid on the primitive cell.[36] Phonon calculations were performed with the finite displacement method.[37] Only Γ-point phonons were calculated so no supercell was used.

3. RESULTS AND DISCUSSION

3.1. Raman Spectroscopy. Raman spectra of 3R−$AgFeO_2$ were collected on compression in three separate experiments over the range of 0−17 GPa. A representative spectrum collected at 0.3(5) GPa is shown in Figure 2. The top panel of Figure 3 plots the fitted peak positions for all runs. At low pressures, two peaks are clearly resolved that correspond to the E_g (346 cm^{-1}) and A_{1g} (645 cm^{-1}) vibrational modes of 3R−$AgFeO_2$.[4,38] The displacement vectors of these two vibrational modes are illustrated in Figure 4. The doubly degenerate E_g vibrational mode involves the displacement of oxygen atoms along the *a*-axis (or *b*-axis), while the A_{1g} mode involves the displacement of oxygen atoms along the *c*-axis. The Fe^{3+} and Ag^+ ions can be considered at rest in both modes.

Upon compression, the E_g and A_{1g} modes increase in frequency up to around 6 GPa, at which point both modes display significant changes: the A_{1g} mode begins to soften, while the E_g mode splits into two distinct modes. This behavior is consistent with that observed in other delafossites, including $CuFeO_2$[39] and $CuLaO_2$.[20] The peak splitting in those cases was attributed to a lowering of symmetry that breaks the degeneracy of the E_g mode.

As pressure is increased, the two modes descended from the E_g mode continue to harden with pressure and further separate to a maximum difference of ∼20 cm^{-1} at around 10 GPa. The two modes move closer with further increasing pressure, becoming a single unresolvable peak at around 14 GPa, while the peak descended from the A_{1g} mode continues to soften over this pressure range. After the recombination of the two low-wavenumber modes, the resulting single peak hardens with increasing pressure up to the maximum pressure measured, with the high-wavenumber peak continuing to soften. The A_{1g} peak remains clearly present up to the maximum pressure measured.

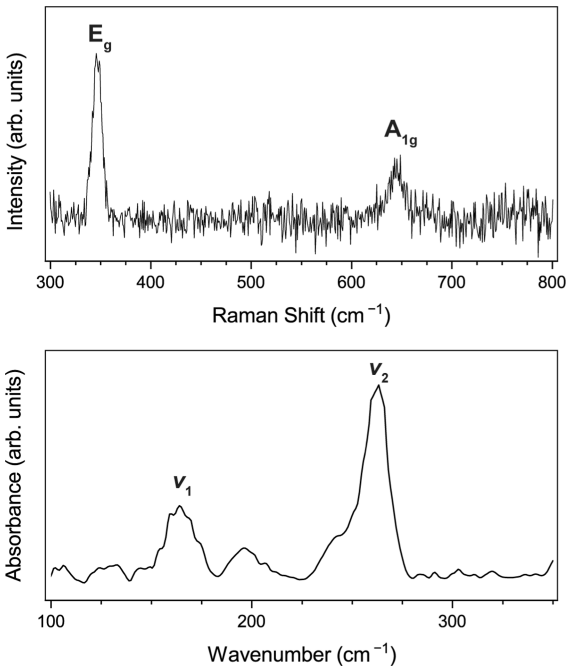

Figure 2. Representative Raman (top) and far-infrared (bottom) spectra collected on the same sample of $AgFeO_2$ at 0.3(5) GPa. Denoted peaks are those whose positions were tracked as a function of pressure. The spectral peak at 195 cm^{-1} —which does not move with pressure—is due to diamond birefringence artifacts inherent to the DAC experiments.

The two discontinuities in the Raman spectra are suggestive of two pressure-induced phase transitions in $AgFeO_2$ appearing at 6 and 14 GPa. Furthermore, the splitting and then recombination of the E_g mode suggests a lowering of symmetry at the first phase transition, followed by a potential recovery of symmetry. In keeping with the literature convention for the delafossites, we will refer to the high-pressure phases as HP1 and HP2.

We calculated the Γ-point phonon modes for the $R\bar{3}m$ structure using density functional theory and found that under a pressure of 4 GPa, the predicted mode frequencies are E_g = 347 cm^{-1} and A_{1g} = 642 cm^{-1}, which agree well with the observed modes.

3.2. Infrared Spectroscopy. For one of our crystals studied with Raman spectroscopy, we also collected far-infrared absorption spectra. A representative spectrum collected at 0.3(5) GPa is plotted in Figure 2. From ambient pressure up to 6 GPa, there are two low-wavenumber features that remain prominent above the background over all pressures and which have a pressure dependence that is consistent with the vibrational modes observed in the Raman spectra. The fitted peak positions of these modes are plotted in the bottom panel of Figure 3.

Using the same Γ-point phonon calculations as used above for interpretation of the Raman spectra, we predict infrared-active low-wavenumber E_u modes at 125 cm^{-1}, an A_{2u} mode at 290 cm^{-1}, E_u modes at 302 cm^{-1}, and an A_{2u} mode at 551

https://doi.org/10.1021/acs.inorgchem.3c04631
Inorg. Chem. 2024, 63, 9763−9770

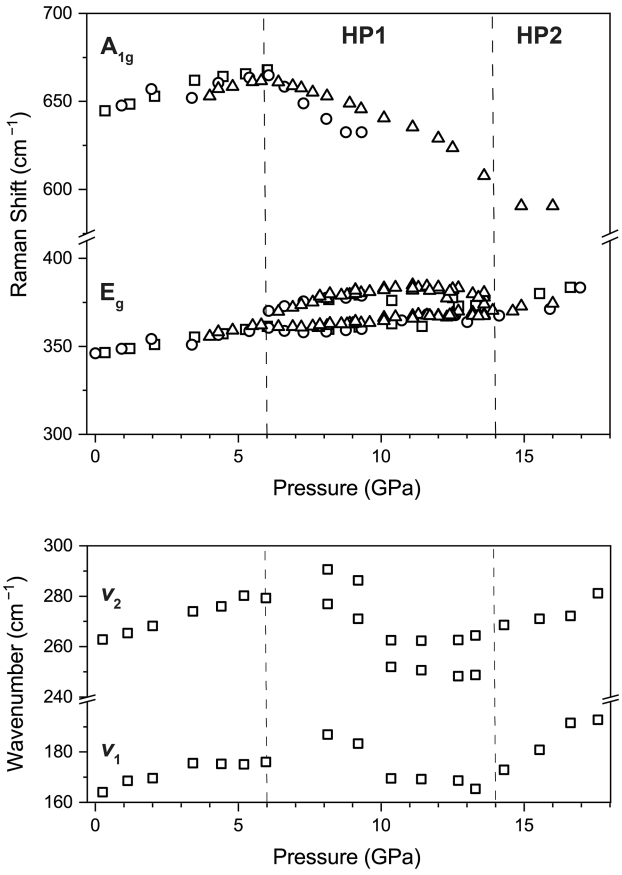

Figure 3. Top: plot of the fitted peak positions in the Raman spectra collected as a function of increasing pressure at 300 K. Different shapes represent data from different crystals. Bottom: plot of the fitted infrared modes selected from the low wavenumber spectra collected at the same pressures as the corresponding Raman spectra above. Dashed lines indicate the pressures at which the total number of resolvable peaks changes, indicating structural phase transitions.

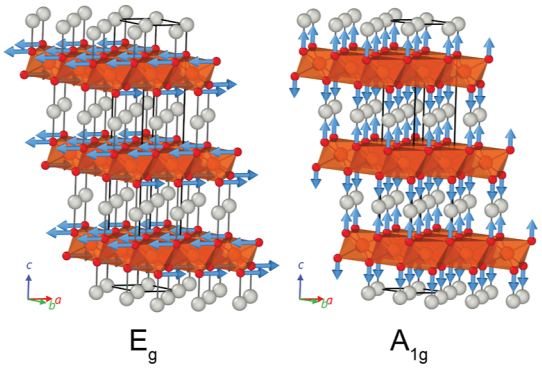

Figure 4. Illustration of displacement vectors describing the two Raman active vibrational modes of 3R−$AgFeO_2$. Blue arrows represent the displacement vectors of the oxygen atoms for each mode with the Fe^{3+} and Ag^+ ions remaining at rest. The vector magnitude is arbitrary and scaled only for clarity.

cm^{-1}. The peak observed experimentally at ∼160 cm^{-1}, which we refer to as ν_1, can be reasonably assigned as E_u. However, the peak at ∼270 cm^{-1} (ν_2) could be either of the A_{2u} or E_u modes. Given that the intensity of absorption is proportional to the square of the changing dipole moment of the mode, we investigated the expected relative intensities by perturbing the structure along the mode eigenvectors and examining the change in partial charges from a Mulliken population analysis. For the same amplitude, the A_{2u} mode changed the Ag−O dipole by 0.01 e, while the E_u mode changed the Ag−O dipole by 0.002 e. This suggests that the intense ν_2 peak is likely from the A_{2u} mode, but further analysis will be required to assign it with confidence.

Below 6 GPa, the two modes harden with pressure at a rate that is consistent with the Raman-active modes. Above 6 GPa, the higher-wavenumber feature clearly splits into at least two separate modes. Between 8−10 GPa, all three modes soften and then level off above ∼11 GPa. At 14 GPa, the two high wavenumber modes appear to merge into a single mode, and the two remaining modes harden up to the maximum pressures reached.

3.3. Brief Summary of Delafossite Polymorphism. A total of nine copper delafossites have been studied previously under pressure, making them the most-studied compounds within this class. The phases studied to date include $CuFeO_2$,[23] $CuGaO_2$,[17] $CuLaO_2$,[20] $CuAlO_2$,[19] $CuInO_2$,[18] $CuYO_2$,[21] $CuMnO_2$,[40] $CuSrO_2$,[41] and $CuCrO_2$.[22] Almost every copper delafossite that has been studied under pressure has been reported to undergo pressure-induced polymorphism into at least one high-pressure polymorph. The exception is $CuMnO_2$, which retains its $C2/m$ structure up to at least 50 GPa.[40] Among the copper delafossites for which phase transitions have been reported, the only systems where crystal structures have been assigned for the high-pressure phases are $CuFeO_2$ and $CuCrO_2$. We briefly review these two phases here.

$CuFeO_2$ has been studied up to 27 GPa using PXRD, Raman spectroscopy, and Mössbauer spectroscopy.[23,39] Two phase transitions have been observed: one at ∼18 GPa (into HP1) and one at ∼27 GPa (into HP2). The structure for HP1 has been assigned as a monoclinic $C2/c$ structure whose interlayer structure can be described as linear O−Cu−O interlayer bonds that are tilted to be nonperpendicular to the $\{FeO_2\}$ slabs. A trigonal $P\bar{3}m$ structure has been assigned for HP2, in which the Ag^+ ions shift into sites with close contact with three oxygen atoms in one slab and one oxygen atom in the other. A charge transfer from (Cu^{1+} $S = 1$, Fe^{3+} $S = 5/2$) to (Cu^{2+} $S = 1/2$, Fe^{2+} $S = 2$) is proposed to occur above 23 GPa. The authors of the structural study comment that confidence in the assigned structures is weakened somewhat by the broadening of the reflections under high pressures.[23] Raman spectroscopy carried out on $CuFeO_2$ complements the XRD, exhibiting a splitting of E_g into two distinct modes at 18 GPa, as well as a softening of the A_{1g} mode after the first phase transition to a monoclinic system.[39]

$CuCrO_2$ has been studied with PXRD and Raman spectroscopy, with a phase transition into an HP1 phase above ∼23 GPa.[22,40] Again, the authors describe a broadening of the diffraction peaks at pressures above 10 GPa that initially obscured a reliable interpretation of the crystal structure of HP1. However, in a more recent study using synchrotron radiation to perform PXRD, HP1 was assigned a $P2_1/m$ structure.[40]

Outside of the copper delafossites, the only other delafossites that have been studied under pressure are $PdCoO_2$,[42] $LiCrO_2$,[43] and $AgGaO_2$.[24] $PdCoO_2$ and $LiCrO_2$ are stable up to at least 10 and 30 GPa, respectively, with no phase transitions being reported in either case.[42] $AgGaO_2$, on the other hand, exhibits two pressure-induced phase transitions at around 10.5 and 16.5 GPa, and PXRD has been used to

https://doi.org/10.1021/acs.inorgchem.3c04631
Inorg. Chem. 2024, 63, 9763−9770

assign structures to both phases.[24] HP1 is assigned as a monoclinic $C2/c$ phase that is analogous to the HP1 phase in $CuFeO_2$, while the HP2 phase is assigned as a trigonal $R\bar{3}m$ phase that can be characterized as having Ag^+ ions in six-coordinate sites between the FeO_2 slabs (the α-$NaFeO_2$ structure).

Returning to $AgFeO_2$, it is interesting that our Raman data closely mirrors that of $CuFeO_2$—albeit at lower pressures—and suggests that the structural transformations may be similar. It is also worth noting that the LP → HP1 transition pressure observed in $AgFeO_2$ (6 GPa) is roughly a third of the pressure observed for $CuFeO_2$ (18 GPa), which is somewhat consistent with the reduced transition pressure of $AgGaO_2$ (10.5 GPa) compared to its copper analogue, $CuGaO_2$ (24 GPa).[24,44]

The reduced transition pressure of the silver systems is likely due to the Ag−O bonds being more compressible than the Cu−O bonds. Indeed, the bulk modulus of $AgGaO_2$ was measured to be 172 GPa,[24] which is lower than the value of 202 GPa measured for the copper analogue.[44] The transition pressure of $AgFeO_2$ being lower than that of $AgGaO_2$ may suggest a relationship that depends upon the B site cation radius—a trend that has been noted for the copper delafossites[45]—but a larger number of compounds will need to be studied before this can be assessed for the silver delafossites.

3.4. X-Ray Diffraction. PXRD data were collected on a powder sample as pressure was increased from 0−16 GPa. A significant broadening of the peaks precluded a reliable indexing of the crystal structure at high pressures (vide supra). The unit cell parameters are plotted up to 6 GPa for the $R\bar{3}m$ phase in the Supporting Information. The c-parameter multiplied by 1.5 of the $C2/c$ phase is plotted between 0−14 GPa. This value is multiplied by 1.5 to keep it comparable with the c-axis of the $R\bar{3}m$ phase. Data points from SCXRD under ambient conditions and 6.3(5) GPa are also included for reference. There is a clear inflection point in the compressibility above 6.0(1) GPa, which agrees with the pressure at which the E_g mode splitting is observed in the Raman spectra (see the Supporting Information).

To determine the HP1 structure, SCXRD experiments were performed in the DAC at 0 GPa and 6.3(5) GPa. The latter pressure was selected to be just above the pressure at which the first transition occurs. The high-pressure crystal structure (HP1) solves in space group $C2/c$. This space group assignment mirrors the previous assignments of HP1 in $AgGaO_2$ and $CuFeO_2$, which were both determined from PXRD data. It should be noted here that attempted structural solutions in space groups $C2/m$ and $P2_1/m$ (other monoclinic space groups that have been reported for high-pressure delafossite phases[24,45,46]) were unsuccessful, with only space group $C2/c$ yielding sensible solutions. We also attempted an analysis of SCXRD data collected at 8.8(5) GPa and 11.1(5) GPa, but a high mosaicity coupled with pressure-induced peak broadening rendered structural solution impossible. Nevertheless, we report here the first a priori structural solution of a high-pressure delafossite phase determined from single-crystal data.

The crystal structure of the $C2/c$ phase is shown in Figure 5. The linear O−Ag−O bonds are tilted to be nonperpendicular with the $\{FeO_2\}$ planes, in contrast with their perpendicular alignment in the 3R−$AgFeO_2$ ambient pressure polymorph. Within a given layer, the O−Ag−O bonds all tilt in the same direction, and the direction of this tilt alternates in every other layer.

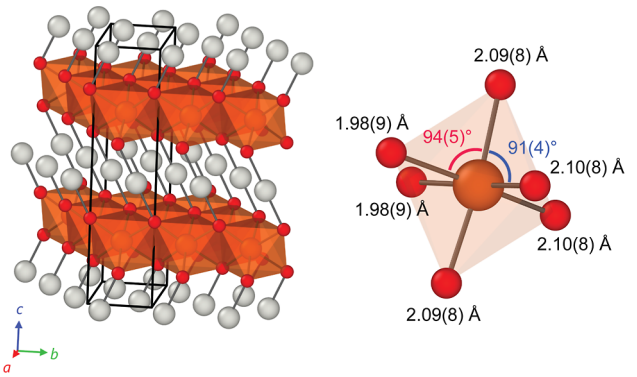

Figure 5. Left: crystal structure of the monoclinic $C2/c$ phase solved from high-pressure single-crystal data collected at 6.3(5) GPa. Right: comparison of Fe−O bond lengths and angles in the $\{FeO_6\}$ octahedra, clearly showing a distorted local environment compared to the 3R−$AgFeO_2$ phase. Colors follow the same scheme outlined in Figure 1.

Analysis of the structure of the high-pressure $C2/c$ phase reveals a distortion of the FeO_6 octahedra relative to the ambient pressure structure (Figure 5). In the low-pressure $R\bar{3}m$ structure, all oxygen sites are equivalent by symmetry and share identical Fe−O bond lengths of 2.035(2) Å. In contrast, the FeO_6 octahedra in the $C2/c$ phase feature three different Fe−O interactions. Two Fe−O bonds of length 2.09(8) Å are near-linear, with an O−Fe−O angle of 175.5°. The other two pairs of symmetrically equivalent Fe−O bond lengths are 2.10(8) Å and 1.98(9) Å and occupy "cis" positions in the $\{FeO_6\}$ octahedron. The observed splitting of the E_g mode in the 6 GPa range can thus be reconciled with this significant local distortion of FeO_6 octahedra and the subsequent loss of symmetry that lifts the mode degeneracy.

3.5. Nuclear Resonant Forward Scattering. NRFS (a.k.a. synchrotron Mössbauer spectroscopy) was performed on 40% ^{57}Fe-enriched 3R−$AgFeO_2$ up to 15.3(5) GPa to track the local electronic environments of the Fe^{3+} sites through the two structural phase transitions. The fitted values of the quadrupole splitting (ΔE_Q) and isomer shift (δ) are plotted in Figure 6.

The ambient pressure Mössbauer parameters of $AgFeO_2$ have been reported elsewhere as δ = 0.37 mm s^{-1} and ΔE_Q = 0.66 mm s^{-1}.[47] The samples used in that study were recovered from a high-pressure synthesis and were characterized as polycrystalline 3R−$AgFeO_2$ mixed with unreacted hematite (Fe_2O_3). Our low-pressure values are consistent with these reported values. ΔE_Q appears to drop at around 6 GPa, which is likely related to local distortions in the $\{FeO_6\}$ octahedra, as detected in the SCXRD performed at 6.3(5) GPa. These distortions would be expected to affecting the symmetry of the local electric field gradient. The magnitude of the drop is smaller than that would be expected if an electronic or magnetic transition had taken place, and indeed, both parameters remain consistent with Fe(III) ions in an S = 5/2 spin state over the entire pressure range.[48,49] We can thus infer that there is no evidence of a charge transfer or spin crossover transition in $AgFeO_2$ up to at least 15.3(5) GPa.

https://doi.org/10.1021/acs.inorgchem.3c04631
Inorg. Chem. 2024, 63, 9763−9770

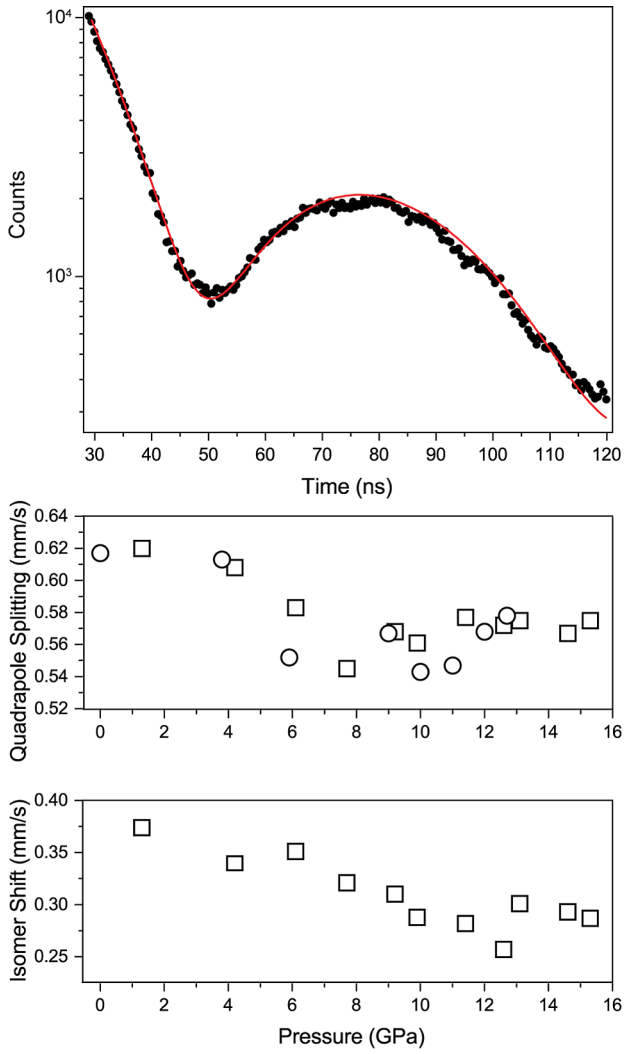

Figure 6. Top: black circles show the NRFS data collected at 0 GPa. The red line shows the fit done by CONUSS that fits the quadrupole splitting as 0.62 mm s^{-1}. Bottom: values of ΔE_Q and δ obtained from fits to the NRFS spectra plotted as a function of pressure. Data from separate experiments are plotted with different shapes.

4. CONCLUSIONS

We have presented the first study of silver ferrite delafossite under high pressures. Two pressure-induced phase transitions were observed in single-crystal samples of the 3R–$AgFeO_2$ polymorph: one at 6 GPa and one at 14 GPa. The two phase transitions were studied using Raman spectroscopy, infrared spectroscopy, XRD, and synchrotron Mössbauer spectroscopy. We assign the first high-pressure polymorph as a monoclinic $C2/c$ structure that is consistent with the high-pressure structures reported for $CuFeO_2$ and $AgGaO_2$. Further studies of silver delafossites with various B-site cations will enable a study of the relationship between the B-site cation radius and the pressures at which the different polymorphs can be accessed.

■ ASSOCIATED CONTENT

Supporting Information

The Supporting Information is available free of charge at https://pubs.acs.org/doi/10.1021/acs.inorgchem.3c04631.

Raman spectra as a function of pressure, temperature, and magnetic field; spectra of infrared data; integrated PXRD patterns; plot of unit cell parameters vs pressure; plots of nuclear resonance forward scattering data; photograph of a sample in the DAC; crystallographic information file for a single crystal of $AgFeO_2$ under ambient conditions; crystallographic information for the $C2/c$ high-pressure phase of $AgFeO_2$; fractional atomic coordinates of $C2/c$ $AgFeO_2$; vibrational modes for 3R–$AgFeO_2$; and all experimental conditions (PDF)

Accession Codes

CCDC 2323507 and 2334053 contain the supplementary crystallographic data for this paper. These data can be obtained free of charge via www.ccdc.cam.ac.uk/data_request/cif, by emailing data_request@ccdc.cam.ac.uk, or by contacting the Cambridge Crystallographic Data Centre, 12 Union Road, Cambridge CB2 1EZ, UK; fax: +44 1223 336033.

■ AUTHOR INFORMATION

Corresponding Authors

Jun Yan – *Department of Physics, University of Massachusetts Amherst, Amherst, Massachusetts 01003, United States;* orcid.org/0000-0003-3861-4633; Email: yan1@umass.edu

James P. S. Walsh – *Department of Chemistry, University of Massachusetts Amherst, Amherst, Massachusetts 01003, United States;* orcid.org/0000-0003-3454-3428; Email: jpswalsh@umass.edu

Authors

Nicholas S. Manganaro – *Department of Chemistry, University of Massachusetts Amherst, Amherst, Massachusetts 01003, United States;* orcid.org/0000-0002-2772-8769

Scott D. Ambos – *Department of Chemistry, University of Massachusetts Amherst, Amherst, Massachusetts 01003, United States;* orcid.org/0000-0001-9898-5626

Matthew DeCapua – *Department of Physics, University of Massachusetts Amherst, Amherst, Massachusetts 01003, United States*

Scott D. Thiel – *Department of Chemistry, University of Massachusetts Amherst, Amherst, Massachusetts 01003, United States;* orcid.org/0000-0002-9947-0277

Wyatt E. Mitchell – *Department of Chemistry, University of Massachusetts Amherst, Amherst, Massachusetts 01003, United States;* orcid.org/0000-0003-2529-4589

Zhenxian Liu – *Department of Physics, University of Illinois Chicago, Chicago, Illinois 60607, United States*

Dongzhou Zhang – *GSECARS, University of Chicago, Lemont, Illinois 60439, United States;* orcid.org/0000-0002-6679-892X

Phuong Q. H. Nguyen – *GSECARS, University of Chicago, Lemont, Illinois 60439, United States*

Barbara Lavina – *GSECARS, University of Chicago, Lemont, Illinois 60439, United States; Advanced Photon Source, Argonne National Laboratory, Lemont, Illinois 60439, United States*

Esen Ercan Alp – *Advanced Photon Source, Argonne National Laboratory, Lemont, Illinois 60439, United States*

Complete contact information is available at: https://pubs.acs.org/10.1021/acs.inorgchem.3c04631

https://doi.org/10.1021/acs.inorgchem.3c04631
Inorg. Chem. 2024, 63, 9763–9770

Notes

The authors declare no competing financial interest.

■ ACKNOWLEDGMENTS

We gratefully acknowledge the University of Massachusetts Amherst for startup funding. This research used beamline 22-IR-1 of the National Synchrotron Light Source II, a U.S. Department of Energy (DOE) Office of Science User Facility operated for the DOE Office of Science by Brookhaven National Laboratory under Contract no. DE-SC0012704. Use of the 22-IR-1 beamline is supported by the National Science Foundation − Earth Sciences via SEES: Synchrotron Earth and Environmental Science (EAR − 2223273) and CDAC (DE-NA0003975). Portions of this work were performed at GSECARS (Sector 13) and Sector 3, Advanced Photon Source (APS), Argonne National Laboratory. Use of the GSECARS gas-loading system and 13-BMC was supported by NSF EAR-1634415 and EAR-1661511. This research used resources of the Advanced Photon Source, a U.S. Department of Energy (DOE) Office of Science user facility operated for the DOE Office of Science by Argonne National Laboratory under Contract No. DE-AC02-06CH11357. B.L. acknowledges the support of COMPRES (EAR-166151). We thank Jasmine Hinton for insightful discussion.

■ REFERENCES

(1) Mao, L.; Mohan, S.; Gupta, S. K.; Mao, Y. Multifunctional delafossite $CuFeO_2$ as water splitting catalyst and rhodamine B sensor. *Mater. Chem. Phys.* **2022**, *278*, 125643.

(2) Harada, T. Thin-film growth and application prospects of metallic delafossites. *Mater. Today Adv.* **2021**, *11*, 100146.

(3) Prevot, M. S.; Jeanbourquin, X. A.; Bouree, W. S.; Abdi, F.; Friedrich, D.; Van De Krol, R.; Guijarro, N.; Le Formal, F.; Sivula, K. Evaluating charge carrier transport and surface states in $CuFeO_2$ photocathodes. *Chem. Mater.* **2017**, *29*, 4952−4962.

(4) Berastegui, P.; Tai, C.-W.; Valvo, M. Electrochemical reactions of $AgFeO_2$ as negative electrode in Li-and Na-ion batteries. *J. Power Sources* **2018**, *401*, 386−396.

(5) Jin, Y.; Chumanov, G. Solution synthesis of pure 2H $CuFeO_2$ at low temperatures. *RSC Adv.* **2016**, *6*, 26392−26397.

(6) Zhang, K. H.; Xi, K.; Blamire, M. G.; Egdell, R. G. P-type transparent conducting oxides. *J. Phys.: Condens. Matter* **2016**, *28*, 383002.

(7) Marquardt, M. A.; Ashmore, N. A.; Cann, D. P. Crystal chemistry and electrical properties of the delafossite structure. *Thin Solid Films* **2006**, *496*, 146−156.

(8) Sheets, W.; Mugnier, E.; Barnabe, A.; Marks, T. J.; Poeppelmeier, K. R. Hydrothermal Synthesis of Delafossite-Type Oxides. *Chem. Mater.* **2006**, *37*, 17−20.

(9) Mackenzie, A. P. The properties of ultrapure delafossite metals. *Rep. Prog. Phys.* **2017**, *80*, 032501.

(10) Jiang, C.-M.; Reyes-Lillo, S. E.; Liang, Y.; Liu, Y.-S.; Liu, G.; Toma, F. M.; Prendergast, D.; Sharp, I. D.; Cooper, J. K. Electronic structure and performance bottlenecks of $CuFeO_2$ photocathodes. *Chem. Mater.* **2019**, *31*, 2524−2534.

(11) Sunko, V.; McGuinness, P.; Chang, C.; Zhakina, E.; Khim, S.; Dreyer, C.; Konczykowski, M.; Borrmann, H.; Moll, P.; König, M.; Muller, D.; Mackenzie, A. Controlled introduction of defects to delafossite metals by electron irradiation. *Phys. Rev. X* **2020**, *10*, 021018.

(12) Barton, P. T.; Seshadri, R.; Knöller, A.; Rosseinsky, M. J. Structural and magnetic characterization of the complete delafossite solid solution $(CuAlO_2)$ 1- x $(CuCrO_2)$ x. *J. Phys.: Condens. Matter* **2012**, *24*, 016002.

(13) Shi, Z.; Wang, T.; Lin, H.; Wang, X.; Ding, J.; Shao, M. Excellent surface-enhanced Raman scattering (SERS) based on $AgFeO_2$ semiconductor nanoparticles. *Nanoscale* **2013**, *5*, 10029−10033.

(14) Dong, X.-D.; Zhao, Z.-Y. Boosting and regulating solar energy conversion performance of delafossite $AgFeO_2$ by spin polarization. *J. Mater. Chem. A* **2022**, *10*, 4800−4816.

(15) Terada, N.; Khalyavin, D. D.; Manuel, P.; Tsujimoto, Y.; Belik, A. A. Magnetic ordering and ferroelectricity in multiferroic 2H-$AgFeO_2$: Comparison between hexagonal and rhombohedral polytypes. *Phys. Rev. B* **2015**, *91*, 094434.

(16) Chuah, X.-F.; Lee, K.-T.; Cheng, Y.-C.; Lee, P.-F.; Lu, S.-Y. Ag/$AgFeO_2$: an outstanding magnetically responsive photocatalyst for HeLa cell eradication. *ACS Omega* **2017**, *2*, 4261−4268.

(17) Pellicer-Porres, J.; Segura, A.; Martínez, E.; Saitta, A.; Polian, A.; Chervin, J.; Canny, B. Vibrational properties of delafossite $CuGaO_2$ at ambient and high pressures. *Phys. Rev. B* **2005**, *72*, 064301.

(18) Jayalakshmi, V.; Murugan, R.; Palanivel, B. Electronic and structural properties of $CuMO_2$ (M= Al, Ga, In). *J. Alloys Compd.* **2005**, *388*, 19−22.

(19) Pellicer-Porres, J.; Segura, A.; Ferrer-Roca, C.; Polian, A.; Munsch, P.; Kim, D. XRD and XAS structural study of $CuAlO_2$ under high pressure. *J. Phys.: Condens. Matter* **2013**, *25*, 115406.

(20) Salke, N. P.; Garg, A. B.; Rao, R.; Achary, S.; Gupta, M.; Mittal, R.; Tyagi, A. Phase transitions in delafossite $CuLaO_2$ at high pressures. *J. Appl. Phys.* **2014**, *115*, 133507.

(21) Cheng, C.; Lv, Z.-L.; Cheng, Y.; Ji, G.-F. Structural, elastic and electronic properties of $CuYO_2$ from first-principles study. *J. Alloys Compd.* **2014**, *603*, 183−189.

(22) Garg, A. B.; Mishra, A.; Pandey, K.; Sharma, S. M. Multiferroic $CuCrO_2$ under high pressure: In situ X-ray diffraction and Raman spectroscopic studies. *J. Appl. Phys.* **2014**, *116*, 133514.

(23) Xu, W.; Hearne, G.; Pasternak, M. $CuFeO_2$ at a megabar: Stabilization of a mixed-valence low-spin magnetic semiconducting ground state. *Phys. Rev. B* **2016**, *94*, 035155.

(24) Chulia-Jordan, R.; Santamaria-Perez, D.; Pellicer-Porres, J.; Otero-de-la-Roza, A.; Martinez-Garcia, D.; Garcia-Domene, B.; Gomis, O.; Sans, J. A.; Vanaja, K.; Asha, A.; Popescu, C. Transition path to a dense efficient-packed post-delafossite phase. Crystal structure and evolution of the chemical bonding. *J. Alloys Compd.* **2021**, *867*, 159012.

(25) Mao, H.; Xu, J.-A.; Bell, P. Calibration of the ruby pressure gauge to 800 kbar under quasi-hydrostatic conditions. *J. Geophys. Res.: Solid Earth* **1986**, *91*, 4673−4676.

(26) Klotz, S.; Chervin, J.; Munsch, P.; Le Marchand, G. Hydrostatic limits of 11 pressure transmitting media. *J. Phys. D: Appl. Phys.* **2009**, *42*, 075413.

(27) Tateiwa, N.; Haga, Y. Evaluations of pressure-transmitting media for cryogenic experiments with diamond anvil cell. *Rev. Sci. Instrum.* **2009**, *80*, 123901.

(28) Dolomanov, O. V.; Bourhis, L. J.; Gildea, R. J.; Howard, J. A.; Puschmann, H. OLEX2: a complete structure solution, refinement and analysis program. *J. Appl. Crystallogr.* **2009**, *42*, 339−341.

(29) Sheldrick, G. M. SHELXT−Integrated space-group and crystal-structure determination. *Acta Crystallogr., Sect. A: Found. Adv.* **2015**, *71*, 3−8.

(30) Rivers, M.; Prakapenka, V. B.; Kubo, A.; Pullins, C.; Holl, C. M.; Jacobsen, S. D. The COMPRES/GSECARS gas-loading system for diamond anvil cells at the Advanced Photon Source. *High Pressure Res.* **2008**, *28*, 273−292.

(31) Matsui, M. High temperature and high pressure equation of state of gold. *J. Phys.: Conf. Ser.* **2010**, *215*, 012197.

(32) Prescher, C.; Prakapenka, V. B. DIOPTAS: a program for reduction of two-dimensional X-ray diffraction data and data exploration. *High Pressure Res.* **2015**, *35*, 223−230.

(33) Sturhahn, W. CONUSS and PHOENIX: Evaluation of nuclear resonant scattering data. *Hyperfine Interact.* **2000**, *125*, 149−172.

(34) Clark, S. J.; Segall, M. D.; Pickard, C. J.; Hasnip, P. J.; Probert, M. I. J.; Refson, K.; Payne, M. C. First principles methods using CASTEP. *Z. Kristallogr. Cryst. Mater.* **2005**, *220*, 567−570.

https://doi.org/10.1021/acs.inorgchem.3c04631
Inorg. Chem. 2024, 63, 9763−9770

(35) Bartók, A. P.; Yates, J. R. Regularized SCAN functional. *J. Chem. Phys.* **2019**, *150*, 161101.
(36) Monkhorst, H. J.; Pack, J. D. Special points for Brillouin-zone integrations. *Phys. Rev. B* **1976**, *13*, 5188−5192.
(37) Frank, W.; Elsässer, C.; Fähnle, M. Ab initio Force-Constant Method for Phonon Dispersions in Alkali Metals. *Phys. Rev. Lett.* **1995**, *74*, 1791−1794.
(38) Ahmed, J.; Alhokbany, N.; Husain, A.; Ahmad, T.; Khan, M. A. M.; Alshehri, S. M. Synthesis, characterization, and significant photochemical performances of delafossite $AgFeO_2$ nanoparticles. *J. Sol-Gel Sci. Technol.* **2020**, *94*, 493−503.
(39) Salke, N. P.; Kamali, K.; Ravindran, T.; Balakrishnan, G.; Rao, R. Raman spectroscopic studies of $CuFeO_2$ at high pressures. *Vib. Spectrosc.* **2015**, *81*, 112−118.
(40) Levy, D.; Greenberg, E.; Layek, S.; Pasternak, M.; Kantor, I.; Pascarelli, S.; Marini, C.; Konopkova, Z.; Rozenberg, G. K. High-pressure structural and electronic properties of $CuMO_2$ (M= Cr, Mn) delafossite-type oxides. *Phys. Rev. B* **2020**, *101*, 245121.
(41) Gilliland, S.; Pellicer-Porres, J.; Segura, A.; Muñoz, A.; Rodríguez-Hernández, P.; Kim, D.; Lee, M.; Kim, T. Electronic structure of $CuAlO_2$ and $CuScO_2$ delafossites under pressure. *Phys. Status Solidi (b)* **2007**, *244*, 309−314.
(42) Hasegawa, M.; Tanaka, M.; Yagi, T.; Takei, H.; Inoue, A. Compression behavior of the delafossite-type metallic oxide $PdCoO_2$ below 10 GPa. *Solid State Commun.* **2003**, *128*, 303−307.
(43) Garg, A. B.; Errandonea, D.; Pellicer-Porres, J.; Martinez-Garcia, D.; Kesari, S.; Rao, R.; Popescu, C.; Bettinelli, M. $LiCrO_2$ under pressure: In-situ structural and vibrational studies. *Crystals* **2018**, *9*, 2.
(44) Pellicer-Porres, J.; Segura, A.; Ferrer-Roca, C.; Martinez-Garcia, D.; Sans, J.; Martinez, E.; Itié, J. P.; Polian, A.; Baudelet, F.; Muñoz, A.; Rodríguez-Hernández, P.; Munsch, P. Structural evolution of the $CuGaO_2$ delafossite under high pressure. *Phys. Rev. B* **2004**, *69*, 024109.
(45) Garg, A. B.; Rao, R. Copper delafossites under high pressure—A brief review of XRD and Raman spectroscopic studies. *Crystals* **2018**, *8*, 255.
(46) Xu, W.; Rozenberg, G. K.; Pasternak, M.; Kertzer, M.; Kurnosov, A.; Dubrovinsky, L.; Pascarelli, S.; Munoz, M.; Vaccari, M.; Hanfland, M.; et al. Pressure-induced Fe ↔Cu cationic valence exchange and its structural consequences: High-pressure studies of delafossite $CuFeO_2$. *Phys. Rev. B* **2010**, *81*, 104110.
(47) Sobolev, A.; Rusakov, V.; Moskvin, A.; Gapochka, A.; Belik, A.; Glazkova, I.; Akulenko, A.; Demazeau, G.; Presniakov, I. ^{57}Fe-enriched Mössbauer study of unusual magnetic structure of multiferroic 3R-$AgFeO_2$. *J. Phys.: Condens. Matter* **2017**, *29*, 275803.
(48) Fultz, B. Mossbauer Spectrometry. In *Characterization of Materials*; Kaufmann, E., Ed.; John Wiley: New York, 2011; .
(49) Pápai, M.; Vankó, G. On Predicting Mössbauer Parameters of Iron-Containing Molecules with Density-Functional Theory. *J. Chem. Theory Comput.* **2013**, *9*, 5004−5020.

https://doi.org/10.1021/acs.inorgchem.3c04631
Inorg. Chem. 2024, 63, 9763−9770